AGU PUBLICATIONS

Geophysical Research Letters

RESEARCH LETTER
10.1002/2014GL060239

Key Points:
- The Chinese loess grain size shows strong 41,000 year cycle during 415–50 ka
- The strong 41,000 year cycle responds to 50°N integrated winter insolation
- The 50°N integrated winter insolation plays a great role in the Asian climate

Supporting Information:
- Readme
- Figure S1
- Figure S2
- Figure S3
- Figure S4
- Figure S5
- Figure S6
- Figure S7
- Figure S8
- Text S1
- Table S1
- Table S2
- Table S3

Correspondence to:
X. Liu,
xliu@lzu.edu.cn

Citation:
Chen, J., X. Liu, and V. A. Kravchinsky (2014), Response of the high-resolution Chinese loess grain size record to the 50°N integrated winter insolation during the last 500,000 years, *Geophys. Res. Lett.*, *41*, doi:10.1002/2014GL060239.

Received 30 MAY 2014
Accepted 13 AUG 2014
Accepted article online 17 AUG 2014

Response of the high-resolution Chinese loess grain size record to the 50°N integrated winter insolation during the last 500,000 years

Jiasheng Chen[1,2], Xiuming Liu[1,3], and Vadim A. Kravchinsky[2]

[1]Key Laboratory of Western China's Environmental Systems, Research School of Arid Environment and Climate Change, Lanzhou University, Lanzhou, China, [2]Department of Physics, University of Alberta, Edmonton, Alberta, Canada, [3]School of Geographical Sciences, Fujian Normal University, Fuzhou, China

Abstract The global ice volume change regulates the Earth's climate and has been characterized by 100,000 year cycles over the last 700,000 years. The Asian inland winter climate change is proposed to show primary 100,000 year cycles that mimic ice volume changes. Here we calibrate the age of a high-resolution grain size record over the last 500,000 years with a grain size age model. The results show a primary 41,000 year cycle and a weaker 100,000 year cycle during the last ~ 500,000 years. We suggest that the primary 41,000 year cycle in the grain size record can be ascribed to the 50°N integrated winter insolation. Our findings suggest that ice volume changes have a limited effect on the Asian inland winter climate. Asian continental winter climate changes respond to the 50°N integrated winter insolation in addition to ice volume changes.

1. Introduction

Wind-blown loess covers an area of about 440,000 km^2 on the Loess Plateau in north central China. Loess is transported from the inland deserts of northwestern China to the Loess Plateau by the northwestern East Asian winter monsoon (Figure S1 in the supporting information). The strong winter monsoon carries coarse loess grains to the Chinese Loess Plateau [*Liu and Ding*, 1998], and the strength of the East Asian winter monsoon can be reconstructed by studying median grain size variations in the loess on the Chinese Loess Plateau [*Porter and An*, 1995]. The Siberian High, centered at 50°N/100°E, has a direct and significant influence on the surface air temperature and the East Asian winter monsoon [*Liu and Ding*, 1998; *Gong et al*., 2001; *Wu and Wang*, 2002; *Hao et al*., 2012] (Figure 1). In summer, the Siberian High disappears (Figure S2a in the supporting information), and the East Asian summer monsoon from the Pacific Ocean in the southeast brings precipitation to the Chinese Loess Plateau (Figure S2b in the supporting information), enhancing soil development. The magnetic susceptibility of loess has proven to be an excellent proxy for changes in the East Asian summer monsoon because the loess magnetic susceptibility depends on the number of fine ferromagnetic particles produced during soil formation [*Zhou et al*., 1990; *Liu et al*., 2007]. A high loess grain size indicates cold and dry glacial climate and corresponds to a high accumulation of loess [*Ding et al*., 2001]. A high magnetic susceptibility corresponds to a relatively warm and humid interglacial climate and to a condition of well-developed paleosols on the central Chinese Loess Plateau [*Zhou et al*., 1990; *Liu et al*., 2007].

The Milankovitch theory suggests that the intensity of solar radiation received by the Earth is paced by Earth's orbital parameters eccentricity, obliquity, and precession, with the commonly referred to periodicities of 100, 41, and 23 thousand years (kyr), respectively [*Milankovič*, 1941]. The 41 kyr obliquity cycle dominates climatic rhythms before the middle Pleistocene transition (1250–700 ka), and the 100 kyr eccentricity cycle dominates in the high latitudinal ice volume and CO_2 records after the middle Pleistocene transition [*Clark et al*., 1999; *Petit et al*., 1999; *Clark et al*., 2006]. The low latitudinal stalagmite $\delta^{18}O$ record reflects the precession cycle for the past 500 kyr and is regulated by changes in summer insolation [*Cruz et al*., 2005; *Wang et al*., 2008; *Cheng et al*., 2012]. The cyclicity of midlatitude climate change reveals the climatic interactions between latitudes. The grain size records, dated by tuning them to Earth's presumed orbital cycles and ice volume changes, show a dominant 100 kyr cycle; thus, grain size was proposed to be regulated by the Northern Hemisphere ice sheet [*Ding et al*., 1995; *Liu and Ding*, 1998; *Sun et al*., 2010; *Hao et al*., 2012]. The newly tuned climate record in Lake Baikal, located between the Northern Hemisphere ice sheet and the Chinese Loess Plateau, strongly reflects the Earth's 41 kyr obliquity cycle and the 100 kyr cycle does not

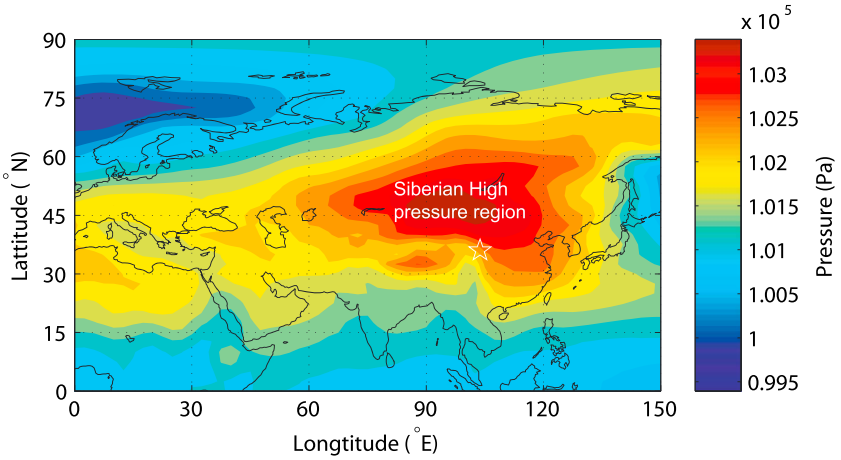

Figure 1. Sea level pressure in January during 1979–2011 and location of JZT section (white star) centered around 50°N. The pressure data are from the National Centers for Environmental Prediction-Department of Energy Reanalysis 2 project at http://www.esrl.noaa.gov/psd/data/gridded/reanalysis/.

constantly prevail over the last 600 kyr [*Kravchinsky et al*., 2003, 2007; *Prokopenko et al*., 2006]. The role of ice volume changes in the East Asian winter monsoon variations remains to be investigated.

Although the high latitudinal insolation-tuned ice volume change and the low latitudinal absolute dated Chinese stalagmite $\delta^{18}O$ record show 100 and 23 kyr cycles, respectively, the times of transition from glacial to interglacial period in both records are highly correlated [*Cheng et al*., 2009], are consistent globally, and are independent of proxies and records. In this study we use (i) the times of transition from glacial to interglacial period as age control points and (ii) the grain size age model built by *Porter and An* [1995] to calibrate the age of grain size variations between the age control points of the Jiuzhoutai (JZT) loess (the thickest loess deposit on the western Chinese Loess Plateau) to calculate the main climatic cyclicity of the East Asian winter climate over the last 500 kyr.

2. Materials and Methods

2.1. Geological Setting and Methodology

The JZT section (36°05′51″*N*, 103°47′11″*E*) in Lanzhou city is situated on the western border of the Chinese Loess Plateau near the Tibetan Plateau (Figure S1 in the supporting information). Its proximity to the Gobi Desert—the inland source of the loess—and its distance from the Pacific Ocean (2000 km) results in a high detritus deposition rate and a low rate of soil development (section 1.1 in Text S1 in the supporting information). Bulk samples from the JZT section were collected every 10 cm to a depth of 120 m and used to analyze two proxy climate parameters—median grain size and magnetic susceptibility (Figure 2).

Three terraces developed in the Huang He River about 600 ka, 120 ka, and 55 ka [*Li et al*., 1997] are possibly linked with the uplift of the northeast Tibetan Plateau [*Li et al*., 1997; *Li and Fang*, 1999]. Tectonic activities in the region are not noted between 600 and 120 ka; therefore, we presume that the grain size variations are regulated solely by climate change in this interval.

2.2. Measurements of Magnetic Susceptibility and Grain Size

Magnetic susceptibility was measured with an MS-2B susceptibility meter (Bartington Instruments) at a sensor frequency of 470 Hz. Grain size was measured using a Mastersizer 2000 analyzer with a size range of 0.02–2000 μm in diameter. Before the grain size analysis, organic material and carbonate formed by pedogenesis was removed with 10% H_2O_2 + 10% HCl, and 0.05 N $(NaPO_3)_6$ was used as a dispersant.

2.3. Age Calibration of the JZT Section

Figure 2a shows the variations in magnetic susceptibility and median grain size versus depth in the studied section. Variations in magnetic susceptibility and grain size in the Xifeng section are comparable to those in other sections on the Chinese Loess Plateau (Figures S3 and S4 in the supporting information). Here we

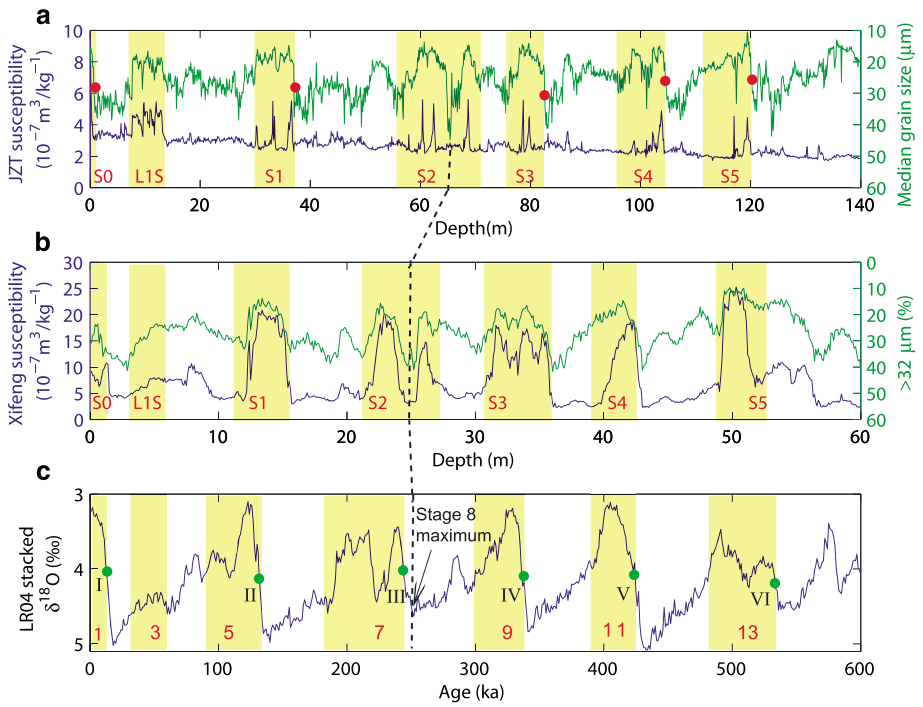

Figure 2. Variations in JZT, Xifeng loess records, and the LR04 stacked benthic $\delta^{18}O$ [*Lisiecki and Raymo*, 2005]. (a) Variations in the JZT median grain size (green line) and magnetic susceptibility (blue line) with depth. Red dots are age control points. (b) Variations in Xifeng median grain size and magnetic susceptibility versus depth from the central Chinese Loess Plateau. The vertical yellow bar and red text in Figures 2a and 2b describe soil units. (c) LR04 stacked benthic $\delta^{18}O$ versus age. The vertical yellow bar and red text denote warm intervals of marine isotope stages. Green dots denote terminations. The black dashed line denotes the glacial maximum of marine isotope stage 8 of the grain size age model suggested.

compare the variations of magnetic susceptibility and grain size in the classic Xifeng section with those in the JZT section. Traditional age models for loess are based on a correlation between high magnetic susceptibility and the warm intervals expressed by lower values of benthic $\delta^{18}O$ [*Kukla*, 1987; *Liu and Ding*, 1998]. In the JZT section, seven soil intervals—S0, L1S, S1, S2, S3, S4, and S5—with high magnetic susceptibility resemble those of the Xifeng section [*Guo et al*., 2009] (Figures 2a and 2b, yellow shadow) and correspond to the marine isotope stages 1, 3, 5, 7, 9, 11, and 13 (Figure 2c, yellow shadow), respectively [*Guo et al*., 2009]. However, the low magnetic susceptibility at 65.4 m in the JZT section and at 25.2 m in the Xifeng section (Figures 2a and 2b) suggests a very cold climate. A cold climate is also supported by the large grain size in the JZT loess and a high content of coarse grains in the Xifeng section. We speculate that the loess samples at 65.4 m in the JZT section and at 25.2 m in the Xifeng section represent severe glacial periods, rather than the subglacial period in marine isotope stage 7 that the traditional age model indicates [*Kukla*, 1987]. The grain size variations in other sections correspond to severe glacial periods in these time intervals as well (Figure S4 in the supporting information).

We used the times of termination in the benthic $\delta^{18}O$ record [*Lisiecki and Raymo*, 2005] to represent the times of transition from glacial to interglacial periods, because the time of each transition is consistent globally in any proxy record. Prominent midpoints between the beginning and the end of the rapid grain size changes that represent transitions from glacial to interglacial periods are used as age control points and correspond to terminations in the benthic $\delta^{18}O$ record (Table S1).

Based on the connections between loess stratigraphy and glacial periods, the midpoints (red dots) in Figure 2a correspond to the terminations [*Lisiecki and Raymo*, 2005] (green dots) in Figure 2c. We do not choose any age control point between S1 and S3 because in our interpretation the maximum grain size at 65.4 m corresponds to a severe glacial interval, most likely the maximum in marine isotope stage 8, which differs from previous age models.

The thickness (120 m) of the JZT loess from the top to S5 (marine isotope stage 13) is more than twice the thickness (50 m) of the loess in the Xifeng section (Figure 2) and other southeast sections (Table S2, Figure S4,

and section 1.1 in Text S1 in the supporting information). This suggests a high loess deposition rate, a strong winter monsoon, and a high-resolution winter monsoon signal in the JZT section. The maximum values of magnetic susceptibility in the JZT section are about one third of those in the Xifeng section and in other southeast sections (Figure S3 in the supporting information). The summer monsoon here is relatively weak. We therefore used grain size variations in the grain size age model [*Porter and An*, 1995] to determine the age of the JZT grain size between age control points.

A high median grain size value [*Porter and An*, 1995] corresponds to an increased capacity of the dust-bearing wind and a higher deposition rate [*Porter and An*, 1995; *Ding et al*., 2001].

$$T_m = T_1 + (T_2 - T_1)\left(\sum_{i=1}^{m} A_i^{-1}\right)\left(\sum_{i=1}^{n} A_i^{-1}\right)^{-1}, \quad (1)$$

where T_m is the calibrated age and T_1 and T_2 are the ages of control points (red points in Figure 2a). A_i is the deposition rate at level (i), which is assumed to be proportional to the median grain size because both are correlated with a strong winter monsoon [*Ding et al*., 2001; *Porter*, 2001]; n is the total sampling level between T_1 and T_2, and m is the sampling level at T_1 and T_2.

2.4. Calculation of Integrated Insolation

To explore the influence of integrated insolation on the JZT grain size record, integrated summer and winter insolation are computed following *Huybers* [2006].

$$J = \sum\nolimits_i \beta_i (W_i \times 86, 400) \quad (2)$$

where J (joules) is integrated insolation, W_i (W/m^2) is the mean insolation on day i, for the calculation of integrated winter insolation—$\beta = 0$ when $W_i \geq \tau$; $\beta = 1$ when $W_i \leq \tau$—and τ (W/m^2) is the daily mean insolation threshold.

Insolation at the top of the atmosphere correlates well with zonally and diurnally averaged land temperatures [*Huybers*, 2006]. A daily mean insolation (W_i) value of 0°C is the daily mean insolation threshold (τ). τ is 275 W/m^2 at 65°N. The ice sheet in the Northern Hemisphere ablates when the 65°N $W_i \geq 275$ W/m^2, a condition that mostly occurs in the summer. *Huybers* [2006] used the sum of $W_i \geq 275$ W/m^2 as the 65°N integrated summer insolation.

The Siberian High develops during the winter and disappears in the summer. It has direct and significant influence on the East Asian winter monsoon. We assume the Siberian High is associated with temperatures lower than 0°C. The Siberian High is centered at 50°N where τ is 250 W/m^2. We suggest that the 50°N integrated winter insolation is the sum of $W_i \leq 250$ W/m^2.

3. Results

Figure 3a shows the relationship between the JZT section depth and the established age (blue) and their fitting curve (red). The grain size age model suggests that the age at depth 65.4 m is 253 ka, which corresponds to the age of the glacial maximum of marine isotope stage 8 in benthic $\delta^{18}O$ records which is 252 ka (Figure 2, black dashed line).

We also calculated a linear interpolated age of the JZT loess section (age at depth 120.1 m (533 kyr)/120.1 m × depth (m)). Figure 3b demonstrates the result of a spectral analysis of the JZT grain size. The four spectral density peaks are close to 100, 41, 23, and 19 kyr Milankovitch cycles. The spectral density of the 41 kyr obliquity cycle is more prominent than the other cycles in the JZT section.

Figure 3c compares the JZT grain size versus age with obliquity cycle variations. From 400 to 50 ka, the grain size correlates positively with Earth's obliquity cycle record. These results illustrate that the obliquity cycle had a strong effect in the JZT section. The phase relationship between the JZT grain size and the obliquity cycle is ambiguous at 50–0 and 550–400 ka (gray shadow in Figure 3c), wherein the JZT grain size rises and falls as the ice volume changes during these two intervals (Figure S5 and section 1.2 in Text S1 in the supporting information).

A wavelet analysis [*Torrence and Compo*, 1998] of the JZT grain size time series reflects the 23 kyr precession cycle only around 410 ka and 250 ka (Figure 3d). The 41 kyr obliquity cycle is well pronounced and continuous

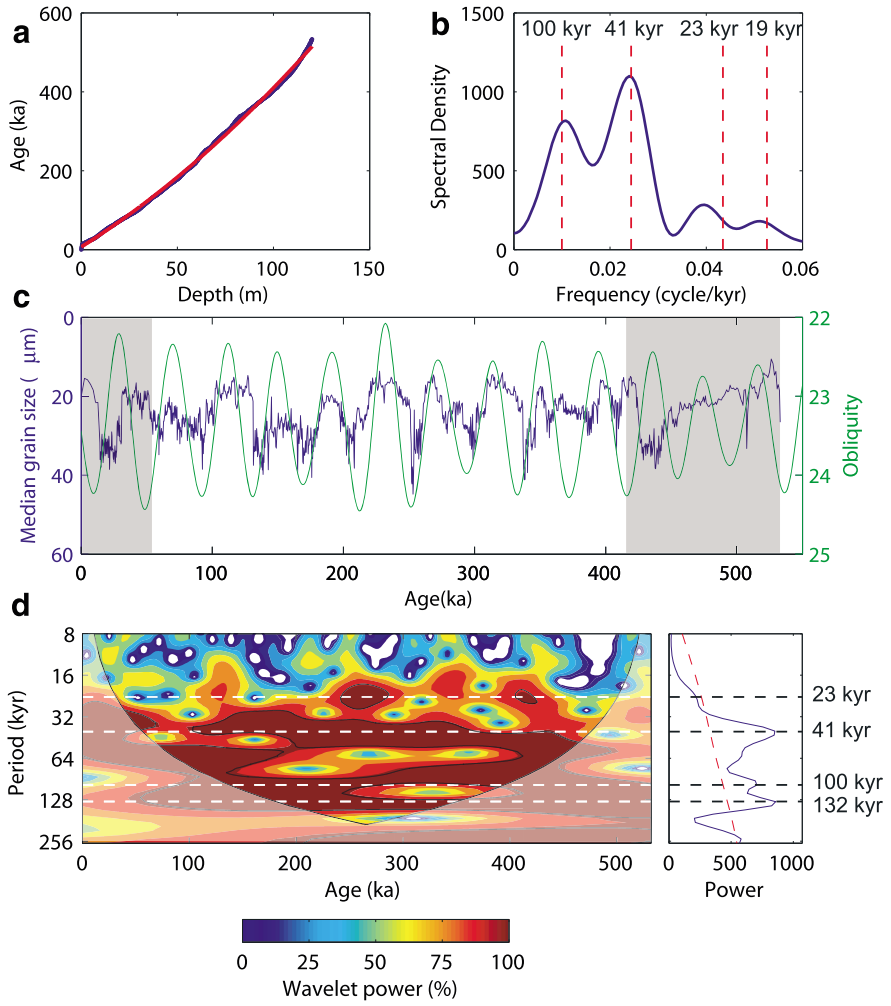

Figure 3. Calibrated age of JZT median grain size. (a) Correlation between calibrated age and depth of the JZT section. The blue line is age versus depth and the red line is the age-depth fitting curve: age = 0.0098 × depth^2 + 3.0478 × depth + 6.699, R^2 = 0.999. (b) Spectral analysis of JZT grain size versus linear interpolated age. (c) Variations of JZT grain size versus age (blue line) and obliquity cycle (green line). Both records do not correlate well at the intervals highlighted by gray vertical bars. (d) The wavelet power spectrum of JZT grain size versus age. Four dashed lines mark the 23 kyr, 41 kyr, 100 kyr, and 132 kyr Milankovitch cycles.

from 450 to 0 ka. The 100 and 132 kyr cycles appear at 533–50 ka. The periodogram illustrates that the 41 kyr obliquity cycle has the largest amplitude over the last 500 kyr. The amplitudes of both 100 and 132 kyr cycles are slightly weaker than that of the 41 kyr cycle. The 132 kyr cycle arises from the frequency modulation of the 100 kyr signal with a longer period 413 kyr component [*Rial*, 1999] (1/100 − 1/413 = 1/132).

The 41 kyr obliquity cycle dominates the global oxygen isotope record from 3 Ma to 0.8 Ma, which is usually ascribed to the summer insolation gradient between high and low latitudes [*Raymo and Nisancioglu*, 2003; *Davis and Brewer*, 2009], e.g., the 65–30°N summer insolation intensity on June 20, or the 65°N integrated summer insolation [*Huybers*, 2006; *Huybers and Tziperman*, 2008]. The East Asian winter monsoon is influenced by the Siberian High centered at 50°N [*Liu and Ding*, 1998; *Gong et al*., 2001; *Wu and Wang*, 2002; *Hao et al*., 2012]; therefore, the 50°N integrated winter insolation, which is dominated by the 41 kyr obliquity cycle, was also calculated (Figure S6 and section 1.2 in Text S1 in the supporting information). From 415 to 50 ka, the JZT grain size correlates positively with both the 65–30°N insolation difference and the 65°N integrated summer insolation and negatively with the 50°N integrated winter insolation (Figure 4). In addition, the JZT grain size appears to match very well with the 50°N integrated winter insolation in detail during the highlighted intervals. Cross correlation confirms that the JZT grain size variations match with the 50°N integrated winter insolation from 415 to 50 ka (Figure S7 in the supporting information). The 50°N

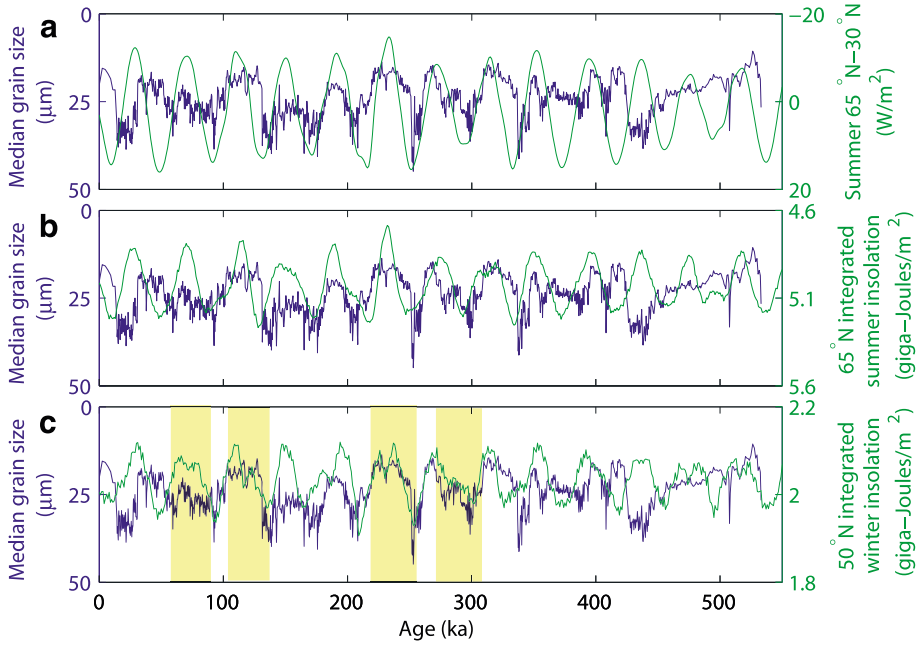

Figure 4. Variations in JZT grain size and insolation. (a) Grain size and summer insolation difference between 65°N and 30°N. (b) Grain size and 65°N integrated summer insolation. (c) Grain size and 50°N integrated winter insolation. The vertical yellow bars in Figure 4c mark similar subtle variations between JZT grain size and integrated winter insolation.

integrated winter insolation appears to be the primary driving force of the strong correspondence between the Earth's obliquity cycle and the 36°N JZT grain size record from 415 to 50 ka. Moreover, the three magnetic susceptibility peaks at depths 60.4 m, 62.4 m, and 68.7 m follow the variations of the 50°N integrated winter insolation (Figure S8 and section 1.3 in the supporting information).

4. Discussion and Conclusions

Although the 100 kyr cycle dominates the ice volume record over the last 500 kyr (Figure S6 in the supporting information), the change in eccentricity is considered to be too small (less than 1%) to cause ice ages [*Imbrie et al*., 1993]. The 100 kyr cycle is, however, ascribed to changes in the ice volume [*Clark et al*., 1999; *Clark et al*., 2006]. The amplitudes of 100 kyr and 132 kyr cycles are prominent in the JZT section (Figure 3d) and the variations in JZT grain size resemble the ice volume record during 50–0 and 550–415 ka intervals. Both features indicate that the ice volume change had an impact on the JZT grain size variations. The increase in ice volume indicates the expansion of ice sheets which cool the air at high latitudes, and the cold air extends to the Siberian region, enhancing the Siberian High, strengthening the East Asian winter monsoon, and bringing coarser grain size sediment to the Chinese Loess Plateau [*Ding et al*., 1995; *Liu and Ding*, 1998; *Hao et al*., 2012].

The obliquity cycle does not change the total amount of solar radiation received by the Earth, but it alters the amplitude of the seasonal cycle, especially at high latitudes [*Milankovič*, 1941]. We suggest that an increase in the obliquity angle results in a decrease in the winter radiative flux from the Sun in both hemispheres, which decreases the 50°N integrated winter insolation and the winter temperatures. Low winter temperatures enhance the Siberian High and drive the East Asian winter monsoon which brings coarse grain size sediments to the Chinese Loess Plateau; therefore, the JZT grain size record responds to the 50°N integrated winter insolation. The presence of a strong obliquity cycle in the climate records of Lake Baikal over the last 600 kyr [*Kravchinsky et al*., 2003, 2007; *Prokopenko et al*., 2006] supports connections among Earth's obliquity cycles, the Siberian High, the East Asian winter monsoon, and the loess grain size variations.

Both the Arctic weather and the Siberian High influence the winter weather on the Asian continent, as reflected in meteorological records [*Gong et al*., 2001; *Wu and Wang*, 2002], which implies that ice volume and

50°N integrated winter insolation can act in concert to influence the East Asian winter climate. The relative strengths of the ice volume and the 50°N integrated winter insolation determine which plays a decisive role in East Asian winter climate variations. The pteridophytes spore content at the Ocean Drilling Program site 646 off southern Greenland during marine isotope stages 11, 9, and 5 is a hundred times higher than that existing during other interglacial periods over the last million years. The abundant spruce pollen content of sediment cores from the site suggests that boreal coniferous forests developed during marine isotope stage 11 and that Greenland was nearly ice free during that time [*De Vernal and Hillaire-Marcel*, 2008]. We suggest that the Greenland ice retreat during 415–50 ka minimized the role of the Arctic ice volume in the East Asian winter climate; the winter climate thus mainly responded to the 50°N integrated winter insolation and thus strongly reflects Earth's obliquity cycles.

The 41 kyr obliquity cycle prevails in ice volume changes, CO_2 variations, and other climate records before the middle Pleistocene transition and is overtaken by the 100 kyr obliquity cycle after the transition [*Clark et al*., 1999; *Petit et al*., 1999; *Clark et al*., 2006]. However, the magnetic susceptibility variations in Alaskan loess strongly reflect Earth's obliquity cycles over the last 250 kyr [*Begét and Hawkins*, 1989]. The climate records at Lake Baikal [*Kravchinsky et al*., 2003, 2007; *Prokopenko et al*., 2006] and our JZT grain size variations strongly reflect the 41 kyr obliquity cycle over the last 500 kyr. We suggest that the 41 kyr obliquity cycle plays a greater role in high and middle latitudinal continental climate change after the middle Pleistocene transition. We demonstrate that the strong 41 kyr cycle in the JZT grain size record can be ascribed to the 50°N integrated winter insolation change. Therefore, we suggest that, in addition to the influence of the 65–30°N summer insolation and the 65°N integrated summer insolation, the 50°N integrated winter insolation contributed to the obliquity cycle signals observed in the Quaternary climate records.

The paleoclimate changes documented by loess sequences have always been considered to follow polar ice core and deep sea $\delta^{18}O$ record variations [*Ding et al*., 1995; *Liu and Ding*, 1998; *Balsam et al*., 2005; *Sun et al*., 2006]. Although the polar ice cores and deep sea sediments are dominated by a 100 kyr cycle, our new loess grain size record shows a strong 41 kyr cycle during 415–50 ka, which can be ascribed to the 50°N integrated winter insolation change. We conclude that the Asian continental winter climate change responded to the 50°N integrated winter insolation in addition to ice volume changes during 415–50 ka and that northern hemispheric ice volume changes had a limited effect on the continental climate to the south of 50°N.

Acknowledgments

We thank X.G. Mao, B. Lü, and Q. Chen for their help with the fieldwork and experiments. This work was supported by the National Science Foundation of China (NSFC grants 41210002, 41072124, 40830105, 41021091, 40772109, 40721061, and 41202129) and the University of Alberta in-kind contributions. The China Scholarship Council supported the joint China/Canada PhD. program for JC. The median grain size data can be found in the supporting information. We express our gratitude to the reviewers, M. Craig and M. Dumberry for their constructive comments which improved the manuscript considerably.

The Editor thanks two anonymous reviewers for their assistance in evaluating this paper.

References

Balsam, W., B. Ellwood, and J. Ji (2005), Direct correlation of the marine oxygen isotope record with the Chinese Loess Plateau iron oxide and magnetic susceptibility records, *Palaeogeogr. Palaeoclimatol. Palaeoecol.*, *221*(1), 141–152, doi:10.1016/j.palaeo.2005.02.009.

Begét, J. E., and D. B. Hawkins (1989), Influence of orbital parameters on Pleistocene loess deposition in central Alaska, *Nature*, *337*(6203), 151–153, doi:10.1038/337151a0.

Cheng, H., R. L. Edwards, W. S. Broecker, G. H. Denton, X. Kong, Y. Wang, R. Zhang, and X. Wang (2009), Ice age terminations, *Science*, *326*(5950), 248–252, doi:10.1126/science.1177840.

Cheng, H., P. Zhang, C. Spötl, R. Edwards, Y. Cai, D. Zhang, W. Sang, M. Tan, and Z. An (2012), The climatic cyclicity in semiarid-arid central Asia over the past 500,000 years, *Geophys. Res. Lett.*, *39*, L01705, doi:10.1029/2011GL050202.

Clark, P. U., R. B. Alley, and D. Pollard (1999), Northern Hemisphere ice-sheet influences on global climate change, *Science*, *286*(5442), 1104–1111, doi:10.1126/science.286.5442.1104.

Clark, P. U., D. Archer, D. Pollard, J. D. Blum, J. A. Rial, V. Brovkin, A. C. Mix, N. G. Pisias, and M. Roy (2006), The middle Pleistocene transition: Characteristics, mechanisms, and implications for long-term changes in atmospheric pCO_2, *Quat. Sci. Rev.*, *25*(23), 3150–3184, doi:10.1016/j.quascirev.2006.07.008.

Cruz, F. W., S. J. Burns, I. Karmann, W. D. Sharp, M. Vuille, A. O. Cardoso, J. A. Ferrari, P. L. S. Dias, and O. Viana (2005), Insolation-driven changes in atmospheric circulation over the past 116,000 years in subtropical Brazil, *Nature*, *434*(7029), 63–66, doi:10.1038/nature03365.

Davis, B. A., and S. Brewer (2009), Orbital forcing and role of the latitudinal insolation/temperature gradient, *Clim. Dyn.*, *32*(2-3), 143–165, doi:10.1007/s00382-008-0480-9.

De Vernal, A., and C. Hillaire-Marcel (2008), Natural variability of Greenland climate, vegetation, and ice volume during the past million years, *Science*, *320*(5883), 1622–1625, doi:10.1126/science.1153929.

Ding, Z., T. Liu, N. W. Rutter, Z. Yu, Z. Guo, and R. Zhu (1995), Ice-volume forcing of East Asian winter monsoon variations in the past 800,000 years, *Quat. Res.*, *44*(2), 149–159, doi:10.1006/qres.1995.1059.

Ding, Z., Z. Yu, S. Yang, J. Sun, S. Xiong, and T. Liu (2001), Coeval changes in grain size and sedimentation rate of eolian loess, the Chinese Loess Plateau, *Geophys. Res. Lett.*, *28*(10), 2097–2100, doi:10.1029/2000GL006110.

Gong, D. Y., S. W. Wang, and J. H. Zhu (2001), East Asian winter monsoon and Arctic oscillation, *Geophys. Res. Lett.*, *28*(10), 2073–2076, doi:10.1029/2000GL012311.

Guo, Z., A. Berger, Q. Yin, and L. Qin (2009), Strong asymmetry of hemispheric climates during MIS-13 inferred from correlating China loess and Antarctica ice records, *Clim. Past*, *5*(1), 21–31.

Hao, Q., L. Wang, F. Oldfield, S. Peng, L. Qin, Y. Song, B. Xu, Y. Qiao, J. Bloemendal, and Z. Guo (2012), Delayed build-up of Arctic ice sheets during 400,000-year minima in insolation variability, *Nature*, *490*(7420), 393–396, doi:10.1038/nature11493.

Huybers, P. (2006), Early Pleistocene glacial cycles and the integrated summer insolation forcing, *Science*, *313*(5786), 508–511, doi:10.1126/science.1125249.

Huybers, P., and E. Tziperman (2008), Integrated summer insolation forcing and 40,000-year glacial cycles: The perspective from an ice-sheet/energy-balance model, *Paleoceanography*, *23*, PA1208, doi:10.1029/2007PA001463.

Imbrie, J., A. Berger, E. Boyle, S. Clemens, A. Duffy, W. Howard, G. Kukla, J. Kutzbach, D. Martinson, and A. McIntyre (1993), On the structure and origin of major glaciation cycles 2. The 100,000-year cycle, *Paleoceanography*, *8*(6), 699–735, doi:10.1029/93PA02751.

Kravchinsky, V. A., M. A. Krainov, M. E. Evans, J. A. Peck, J. W. King, M. I. Kuzmin, H. Sakai, T. Kawai, and D. F. Williams (2003), Magnetic record of Lake Baikal sediments: Chronological and paleoclimatic implication for the last 6.7 Myr, *Palaeogeogr. Palaeoclimatol. Palaeoecol.*, *195*(3–4), 281–298, doi:10.1016/S0031-0182(03)00362-6.

Kravchinsky, V. A., M. E. Evans, J. A. Peck, H. Sakai, M. A. Krainov, J. W. King, and M. I. Kuzmin (2007), A 640 kyr geomagnetic and paleoclimatic record from Lake Baikal sediments, *Geophys. J. Int.*, *170*(1), 101–116, doi:10.1111/j.1365-246X.2007.03411.x.

Kukla, G. (1987), Loess stratigraphy in central China, *Quat. Sci. Rev.*, *6*(3–4), 191–219, doi:10.1016/0277-3791(87)90004-7.

Li, J., and X. Fang (1999), Uplift of the Tibetan Plateau and environmental changes, *Chin. Sci. Bull.*, *44*(23), 2117–2124.

Li, J., X. Fang, R. Van der Voo, J. Zhu, C. M. Niocaill, Y. Ono, B. Pan, W. Zhong, J. Wang, and T. Sasaki (1997), Magnetostratigraphic dating of river terraces: Rapid and intermittent incision by the Yellow River of the northeastern margin of the Tibetan Plateau during the Quaternary, *J. Geophys. Res.*, *102*(B5), 10,121–10,132, doi:10.1029/97JB00275.

Lisiecki, L. E., and M. E. Raymo (2005), A Pliocene-Pleistocene stack of 57 globally distributed benthic δ^{18}O records, *Paleoceanography*, *20*, PA1003, doi:10.1029/2004PA001071.

Liu, Q., C. Deng, J. Torrent, and R. Zhu (2007), Review of recent developments in mineral magnetism of the Chinese loess, *Quat. Sci. Rev.*, *26*(3-4), 368–385, doi:10.1016/j.quascirev.2006.08.004.

Liu, T., and Z. Ding (1998), Chinese loess and the paleomonsoon, *Annu. Rev. Earth Planet. Sci.*, *26*(1), 111–145, doi:10.1146/annurev.earth.26.1.111.

Milankovič, M. (1941), *Canon of Insolation and The Ice-Age Problem*, Königlich Serbische Akademie, Beograd, Washington, D. C., English translation by the Israel Prog. for Sci. Translations, 1998.

Petit, J. R., J. Jouzel, D. Raynaud, N. Barkov, J.-M. Barnola, I. Basile, M. Bender, J. Chappellaz, M. Davis, and G. Delaygue (1999), Climate and atmospheric history of the past 420,000 years from the Vostok ice core, Antarctica, *Nature*, *399*(6735), 429–436, doi:10.1038/20859.

Porter, S. C. (2001), Chinese loess record of monsoon climate during the last glacial-interglacial cycle, *Earth Sci. Rev.*, *54*(1–3), 115–128, doi:10.1016/S0012-8252(01)00043-5.

Porter, S. C., and Z. S. An (1995), Correlation between climate events in the North Atlantic and China during the last glaciation, *Nature*, *375*(6529), 305–308, doi:10.1038/375305a0.

Prokopenko, A. A., L. A. Hinnov, D. F. Williams, and M. I. Kuzmin (2006), Orbital forcing of continental climate during the Pleistocene: A complete astronomically tuned climatic record from Lake Baikal, SE Siberia, *Quat. Sci. Rev.*, *25*(23), 3431–3457, doi:10.1016/j.quascirev.2006.10.002.

Raymo, M. E., and K. Nisancioglu (2003), The 41 kyr world: Milankovitch's other unsolved mystery, *Paleoceanography*, *18*(1), 1011, doi:10.1029/2002PA000791.

Rial, J. (1999), Pacemaking the ice ages by frequency modulation of Earth's orbital eccentricity, *Science*, *285*(5427), 564–568, doi:10.1126/science.285.5427.564.

Sun, Y., S. C. Clemens, Z. An, and Z. Yu (2006), Astronomical timescale and palaeoclimatic implication of stacked 3.6-Myr monsoon records from the Chinese Loess Plateau, *Quat. Sci. Rev.*, *25*(1), 33–48, doi:10.1016/j.quascirev.2005.07.005.

Sun, Y., Z. An, S. C. Clemens, J. Bloemendal, and J. Vandenberghe (2010), Seven million years of wind and precipitation variability on the Chinese Loess Plateau, *Earth Planet. Sci. Lett.*, *297*(3), 525–535, doi:10.1016/j.epsl.2010.07.004.

Torrence, C., and G. P. Compo (1998), A practical guide to wavelet analysis, *Bull. Am. Meteorol. Soc.*, *79*(1), 61–78, doi:10.1175/1520-0477(1998)079<0061:APGTWA>2.0.CO;2.

Wang, Y., H. Cheng, R. L. Edwards, X. Kong, X. Shao, S. Chen, J. Wu, X. Jiang, X. Wang, and Z. An (2008), Millennial-and orbital-scale changes in the East Asian monsoon over the past 224,000 years, *Nature*, *451*(7182), 1090–1093, doi:10.1038/nature06692.

Wu, B., and J. Wang (2002), Winter Arctic oscillation, Siberian high and East Asian winter monsoon, *Geophys. Res. Lett.*, *29*(19), 1897, doi:10.1029/2002GL015373.

Zhou, L., F. Oldfield, T. Liu, A. Wintle, S. Robinson, and J. Wang (1990), Partly pedogenic origin of magnetic variations in Chinese loess, *Nature*, *346*(6286), 737–739, doi:10.1038/346737a0.